# Multichannel Conductivity Measurement Equipment for Efficient Thermal and Conductive Characterization of Nonaqueous Electrolytes and Ionic Liquids for Lithium Ion Batteries†

**Hans-Georg Schweiger, Philipp Wachter, Tobias Simbeck, Franz Wudy, Sandra Zugmann, and Heiner Jakob Gores***

Institut für Physikalische und Theoretische Chemie, Universität Regensburg, 93040 Regensburg, Germany

Knowledge of the (specific) conductivities ($\kappa$) of nonaqueous electrolytes and their liquid range are key issues for the development and optimization of lithium ion batteries. Solidification and melting points of ionic liquids (ILs) cannot be determined easily, as ILs show a tendency toward supercooling, especially when high cooling rates are needed to get useful signals. Therefore, we have developed an integrated computer-controlled measurement apparatus that allows the determination of conductivity and solidification or fusion points as functions of temperature simultaneously for up to 30 samples and at very small cooling rates (as low as 1 $K \cdot h^{-1}$). The accuracy of the conductivity measurement equipment was analyzed by the error propagation law and by experiments as well. Over the range 5 $\mu S \cdot cm^{-1}$ to 5 $mS \cdot cm^{-1}$, relative uncertainties of better than 2 % of the measured values were achieved. The relative resolution of the conductivity measurements is better than 0.001 times the measured value. A detailed description of our system, including circuitries and error calculations, is given along with some examples of its application in studying liquid electrolyte solutions and ILs.

## Conductivity Determination for Nonaqueous Electrolytes and Ionic Liquids

The (specific) conductivity ($\kappa$) of easily deformable ion conductors such as electrolyte solutions, gels, ionic liquids (ILs), and polymer electrolytes is a member of the class of transport parameters. $\kappa$ is the best-studied key property for the performance of lithium ion cells. It determines their voltage drop as a function of the flowing current ($I$) and hence their power density as well as their heat evolution during charging and discharging (see eq 1). The cell potential is given by[1]

$$E_{cell} = E_0 - \eta_{ct,A} - \eta_{ct,C} - \eta_{c,A} - \eta_{c,C} - IR_i \quad (1)$$

where $E_0$ is the open-circuit voltage of the cell, $\eta_{ct,A}$ and $\eta_{ct,C}$ refer to the charge-transfer (ct) overpotentials at the cathode (C) and anode (A), respectively, $\eta_{c,A}$ and $\eta_{c,C}$ are the overpotentials caused by the concentration polarization (c) at the electrodes, and $R_i$ is the internal resistance of the cell. This resistance is determined by the conductivity of the selected ion conductor and by the geometry of the cell, which is often called the cell constant, $K_{cell}$. The overpotentials $\eta_{ct,A}$, $\eta_{ct,C}$, $\eta_{c,A}$, and $\eta_{c,C}$ strongly depend on $I$. Knowledge of the heat evolution, mainly given by $IR_i^2$, is especially important for large lithium ion batteries (LIBs), as it may adversely affect their performance.[2]

Since the start of our studies in the late 1960s, generally very precise measurements have been conducted for electrolyte solutions from vanishing concentrations of salts up to saturation over the temperature range from (228 to 303) K and later extended up to 408 K. The information on ion−ion and ion−solvent interactions thus obtained has been used to optimize the conductivity at high concentrations of the salt[3] in electrolyte solutions.

The temperature dependence of diluted electrolyte solutions has been determined by recording conductivities at selected constant temperatures in steps of several degrees over a given temperature range. After the content of salt in the electrolyte solution was increased, this procedure was repeated.

Concentrated solutions with preselected high salt contents have been measured using up to 10 conductivity cells at a time over a selected temperature range.[4] Such measurements are very time-consuming and only reasonable if high-precision data with uncertainties of 0.01 % are required. For electrolyte optimization studies, much lower precision is sufficient, and automated measurement equipment such as that presented in this article can be used.

The conductivity of a typical electrolyte solution containing varying contents of lithium salts, organic solvents, and other additives is a function of composition as well as temperature.[3] Therefore, optimization of conductivity is very time-consuming, as the number of required measurements strongly increases with the number of components. To find a remedy, we recently introduced a procedure guided by the simplex algorithm to reduce the number of necessary measurements (for details see refs 5 and 6).

ILs and their blends were recently introduced as substitutes for organic solvents in lithium ion batteries, as they offer very low vapor pressures and thus increase the security of LIBs.[7] Optimization of electrolytes based on blends of ILs and one or more lithium salts has just started in our laboratories. The automated measurement equipment presented herein and the optimization of conductivities guided by the simplex algorithm are both being used. At low temperatures, solvents may solidify or salts may reach their solubility limit. Our automated

† Part of the "Josef M. G. Barthel Festschrift".

* Corresponding author. Tel.: +49(0)941/9434746. Fax: +49(0)941 /9434532. E-mail: heiner.gores@chemie.uni-regensburg.de.

10.1021/je900942f 
Published on Web 01/19/2010

measurement equipment presented here can determine the liquid range and solubility limits of those electrolytes very effectively.

The significance of the method can further be increased by simultaneously measuring the temperature within the conductivity cell. Both $\kappa(t)$ and $T(t)$ show typical indications when a solvent solidifies or a salt precipitates from the solution, even at very small cooling or heating rates. Our multichannel conductivity measurement equipment, which is able to perform both tasks, is described in this paper. With this equipment, simultaneous measurements of temperature-dependent conductivities of electrolyte solutions and the detection of phase transitions of conducting solutions are possible. As a large number of samples have to be analyzed during battery electrolyte optimization, a multichannel apparatus was built.

Typical nonaqueous electrolytes show conductivities in the range (0.1 to 100) $mS \cdot cm^{-1}$.[3] When measurements are performed at very low temperatures, it is necessary to measure even lower conductivities (as low as 1 $\mu S \cdot cm^{-1}$). If phase transitions in electrolyte solutions or ILs are investigated, a relative resolution of about 0.001 times the measured value is needed. To ensure that thermal equilibrium is maintained during the measurement, only low temperature change rates, in the range (1 to 10) $K \cdot h^{-1}$, are used. Therefore, only 1 to 10 measurements per second are needed.

It should be stressed that the determination of thermodynamic equilibrium points such as fusion points (zero degrees of freedom at constant pressure) is generally performed using small samples [(10 to 20) mg] with differential thermal analysis or differential thermal calorimetry. However, small samples entail impurity effects, have no room for crystallization aids, and need a rather high temperature change rate [(5 to 20) $K \cdot min^{-1}$]. As a consequence of this nonequilibrium situation, the values obtained are subject to deviations, especially when supercooling plays a role, as is often observed for ILs. We therefore selected cells with a far larger volume, allowing the use of very low temperature change rates (down to about 1 $K \cdot h^{-1}$) and providing enough room for crystallization aids. In addition, as the equipment presented here is a computer-coupled automated system, runs are easily repeated.

## Apparatus for Measuring Temperature-Dependent Conductivities

The equipment was designed to measure conductivity and temperature for a set of cells (up to 30) simultaneously. For these measurements, a temperature-controlled oil bath provides linear changes to the temperature of the samples with time. Stirring equipment ensures homogenization of the samples. The conductivities and temperatures of the samples inside the cells are measured simultaneously using a home-built multichannel thermometer and multichannel conductivity meter. A detailed description of this in-house-built equipment and the results of the error analysis and a noise study are given in the Supporting Information.

***Calibration.*** The design of the cells does not ensure the stability of the cell constants when electrolytes are changed. Cleaning the cells may slightly change the geometry of the electrodes because the stirring bar touches the electrodes when it is removed during cleaning. The cell constant is also dependent on the volume of electrolyte inside the cell. Therefore, the cell constant $K_{cell}$ has to be determined every time the electrolyte is changed. This is performed by measuring $\kappa$ for the electrolyte using cells with known cell constants at a fixed temperature. The $K_{cell}$ value for the new cell is determined using the following equation:

$$K_{cell} = \frac{\kappa}{G} \tag{2}$$

where $G$ is the conductivity measured using the conductivity meter. For the experiments shown in the Supporting Information, the cells used for calibration were a miniaturized version of cells described in the literature.[4]

***Examples of Application. Electrolyte Solutions.*** The fusion/crystallization point of the electrolyte of a lithium ion battery determines the lower operational temperature of the cell. If the electrolyte freezes or solid salt is precipitated from the electrolyte, a dramatic loss of performance of the cell results. To avoid this problem, every electrolyte should be analyzed prior to application. We optimized the conductivity of various electrolytes based on lithium bis[1,2-oxalato(2−)-*O*,*O*′]borate (LiBOB) in blends of organic carbonates and esters. Details concerning the results of these optimizations and the preparation of samples are described elsewhere.[6] We investigated the liquid range of all the electrolytes described in this article.

Two examples of these measurements to demonstrate the capabilities of the instrument are described here. First, results from $T(t)$ measurements with a previous system[10] alone were given in ref 8, where we also showed that well-studied melting points of pure liquids were correctly found with our equipment. For our thermostat, see the Supporting Information and ref 9.

LiBOB was dissolved in two different mixtures of ethylene carbonate (EC), propylene carbonate (PC), and dimethyl carbonate (DMC). Ethyl acetate was then added to one of the mixtures as an additional solvent to improve the conductivity. The compositions of the electrolytes (the salt molality $m_{LiBOB}$ and the blend composition mass fractions $w_i$) are shown in Table 1. To reduce supercooling, carbon fibers were added as described in literature.[8]

The results of the cooling and heating measurements for electrolyte 1 are shown in Figure 1. The measurements were conducted over the temperature range (291 to 239) K at cooling and heating rates of 6 $K \cdot h^{-1}$.

In the heating experiment, no change in the slope of the $T(t)$ curve was observed. The slight change in the slope of $\kappa(t)$ indicates precipitated electrolyte components at temperatures below 251 K. Because the change of slope was not sharp, no precise information about the transition temperature could be derived.

The $\kappa(t)$ curve from the cooling experiment showed a slight change in slope at about 251 K also. The $T(t)$ curve showed behavior typical of a supercooled liquid at about 245 K. The difference between the $\kappa(t)$ and $T(t)$ curves is explained by the fact that at the beginning of crystallization only a small amount of energy is released, so no effect on the temperature curve was observed.

When only temperature is used as phase transition indicator, as has been done for nonconducting liquids in the literature,[8] there is the danger of not being able to find the correct phase transitions of electrolytes. A more pronounced effect is found when information from the thermometer and the conductivity meter are combined. In Figure 2, the temperature dependences

**Table 1. Composition of the Electrolytes Used for Cooling and Heating Experiments on the Salt LiBOB in a Mixture of Various Carbonates**

| electrolyte | $m_{LiBOB}$ / $mol \cdot kg^{-1}$ | $w_{EC}$ | $w_{PC}$ | $w_{DMC}$ | $w_{EA}$ |
|---|---|---|---|---|---|
| 1 | 0.47 | 0.198 | 0.413 | 0.388 | − |
| 2 | 1.08 | 0.00037 | 0.0437 | 0.0175 | 0.935 |

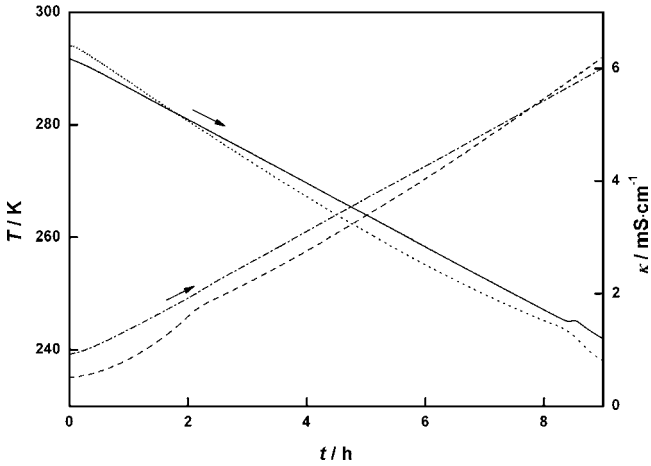


**Figure 1.** Results of cooling and heating experiments using a LiBOB-based electrolyte ($m_{LiBOB} = 0.47$ mol·kg$^{-1}$, $w_{EC} = 0.198$, $w_{PC} = 0.413$, $w_{DMC} = 0.388$). The cooling and heating rates were 6 K·h$^{-1}$. The dot-dashed line shows the temperature of the sample and the dashed line the conductivity of the sample during the heating experiment. The temperature (solid line) and conductivity (dotted line) of the sample during cooling experiments are also shown.

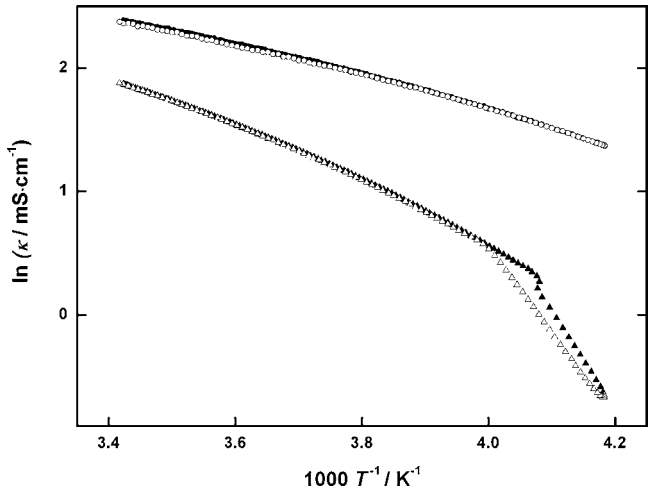


**Figure 2.** Temperature dependence of the specific conductivity over the temperature range (239 to 292) K for LiBOB in EC/PC/DMC/EA (electrolyte 2) (○, heating; ●, cooling) and LiBOB in EC/PC/DMC (electrolyte 1) (△, heating; ▲, cooling).

of the specific conductivities of the two electrolytes are shown in the form of Arrhenius plots.

In this plot, the specific conductivity of electrolyte 1 shows a clear change in slope at 250.7 K in the heating curve and 245 K in the cooling curve. This difference is caused by delayed precipitation of one of the electrolyte components due to supercooling. The specific conductivity of electrolyte 2 shows the typical Vogel−Fulcher−Tammann (VFT) behavior (curved ln $\kappa$ vs 1000·$T^{-1}$ plot), indicating that no phase transition occurs in the investigated temperature range.

***1-Ethyl-3-methylimidazolium tetrafluoroborate ([EMIM][BF$_4$]).*** This IL was a high-purity sample (low water content, no chloride impurity, no impurities detectable by NMR analysis) from previous investigations (for details, see refs 18 and 19). Figure 3 displays the results of heating a crystallized sample of this IL. Both the $T(t)$ and $\kappa(t)$ functions clearly show breaks indicating melting of the sample. The fusion temperature of the sample is obtained from the intersection of the upper and lower parts of the curves. The results of our evaluation (Table 2) were (286.57 ± 0.16) K using the $T(t)$ data and (286.98 ± 0.1) K

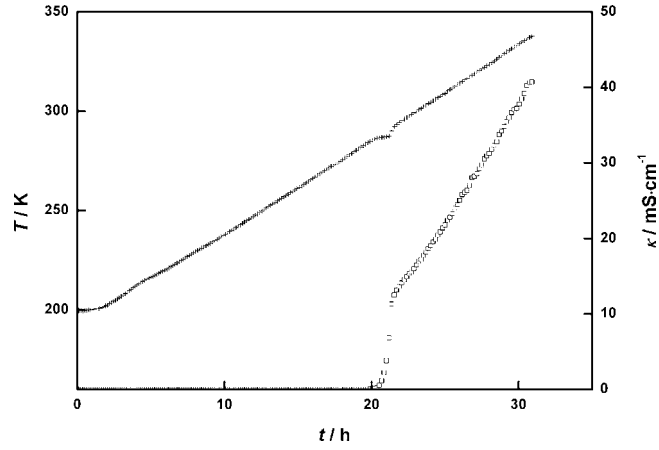


**Figure 3.** Results of heating experiments (heating rate 1 K·h$^{-1}$) on the IL [EMIM][BF$_4$]: +, temperature; □, conductivity. In the figure, only every 20th point is shown.

**Table 2. Melting Points Obtained by Evaluation of $T(t)$ Curves, $T_{fus}[T(t)]$, and by Evaluation of $\kappa(t)$ curves, $T_{fus}[\kappa(t)]$, Along with Melting Points Given in the Literature ($T_{fus,lit}$)**

| | $T_{fus}[T(t)] \pm \Delta T_{fus}$ | $T_{fus}[\kappa(t)] \pm \Delta T_{fus}$ | $T_{fus,lit}$ | |
|---|---|---|---|---|
| IL | K | K | K | reference |
| [EMIM][BF$_4$] | 286.57 ± 0.16 | 286.98 ± 0.1 | 286 | 11 |
| | | | 284 | 12 |
| | | | 287.7 | 13 |
| | | | 288 | 14 |
| | | | 287.57 ± 0.33 | 15 |
| [EMIM][DCA] | 267.75 ± 0.15 | 268.25 ± 0.5 | 261 | 16 |
| | | | 252 | 17 |

using the $\kappa(t)$ data; these are very similar to other values from literature (see Table 2).

***1-Ethyl-3-methylimidazolium dicyanamide ([EMIM][DCA]).*** This IL was a high-purity sample (low water content, no chloride impurity, no impurities detectable by NMR analysis) from previous investigations (for details, see refs 18 and 20). The NMR data for [EMIM][DCA] did not show any impurities, and the water content was determined via Karl Fischer titration to be less than 20 ppm.

The results of heating experiments on [EMIM][DCA] with a low heating rate of 5 K·h$^{-1}$ are presented in Figure 4. The conductivity versus temperature data show a clear effect (a drop in conductivity) caused by the solid−liquid phase transition of

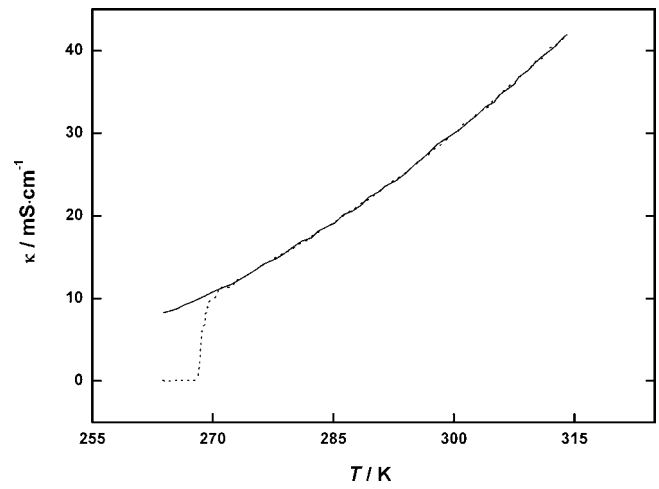


**Figure 4.** Temperature dependence of conductivity of [EMIM][DCA] during heating at 5 K·h$^{-1}$. The solid line shows the VFT fit and the dashed line the measured conductivity.

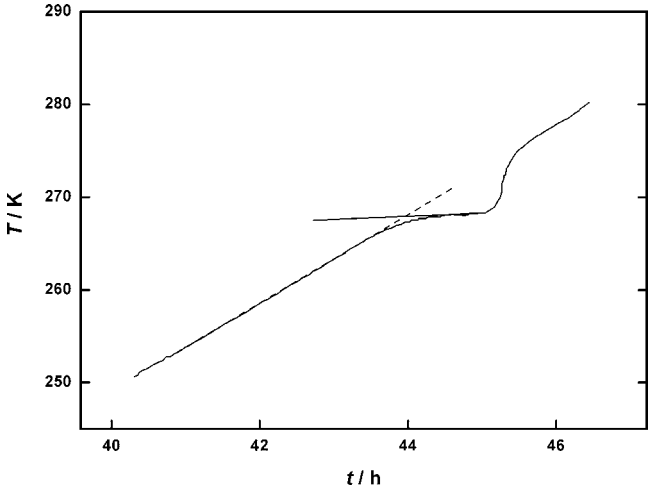


**Figure 5.** Time dependence of the temperature of [EMIM][DCA] during heating at 5 K·h$^{-1}$. The dashed line shows the extrapolation.

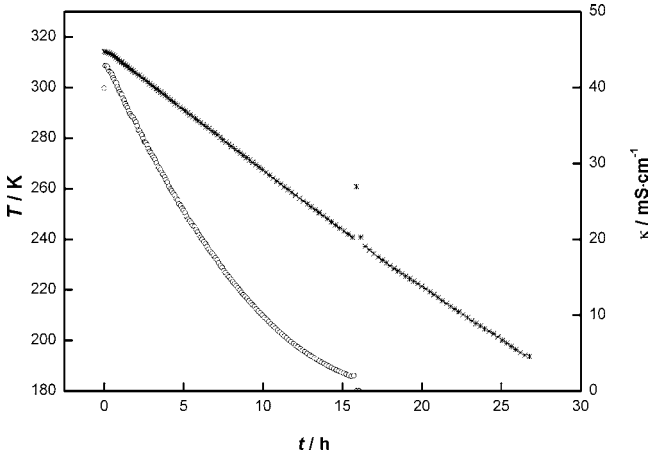


**Figure 6.** Results of cooling experiments (cooling rate 5 K·h$^{-1}$) on the IL [EMIM][DCA]: ∗, temperature; ○, conductivity. In the figure, only every 50th point is shown.

[EMIM][DCA] at (268.25 ± 0.5) K. Data from these measurements are shown in Figure 4. The same data can also be analyzed by classical thermal analysis of the $T(t)$ curve. Figure 5 shows the $T(t)$ curve of the same heating experiment with [EMIM][DCA]. Analysis of the shoulder of the $T(t)$ curve gives a fusion temperature of (267.75 ± 0.15) K. Literature data span a range down to 252 K (see Table 2). We assign the deviations between our data and the literature values to supercooling caused by the fast scan methods used to obtain the latter. This example clearly shows the advantage of low heating rates in determining melting points (if possible).

In contrast, the cooling curves $T(t)$ and $\kappa(t)$ are strongly affected by supercooling, yielding (259.95 ± 2) K and (256 ± 2) K, respectively (see Figure 6) and showing a huge spike of about 20 K in the $T(t)$ function upon solidification of [EMIM][DCA], where the temperature of the sample nearly reached the fusion point (roughly 268 K; see Table 2). Figure 7 shows the effect of supercooling in an experiment where a temperature cycle is shown in the form of an Arrhenius plot. First, the function shows the typical VFT behavior, with a nonlinear Arrhenius plot. Next, as a result of the crystallization heat also seen as the huge spike in Figure 6, the conductivity increases again and then drops to very low values. When the sample is reheated, the equilibrium conductivity is reached near the equilibrium point of [EMIM][DCA] at 268.25 K (also see Figure 4).

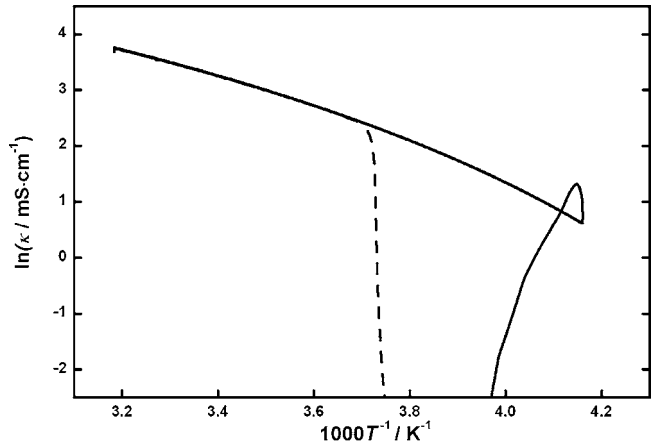


**Figure 7.** Logarithm of the conductivity of [EMIM][DCA] for a temperature cycle, first with cooling and then with heating both at a rate of 5 K·h$^{-1}$. The solid line shows the cooling curve and the dashed line the heating curve. The deviation between the cooling and heating curves is caused by the phase transition from the supercooled liquid to the solid.

## Conclusion

Coupling a multichannel thermometer with a multichannel conductivity meter speeds up the development of electrolytes devices such as lithium ion batteries. With the setup described here, specific conductivities of up to 30 samples can be measured over a broad temperature range automatically under inert gas conditions. Relative uncertainties of 2 % or less are reached in the main area of interest. Because of the high resolution of the thermometer and the conductivity meter, phase transitions of the electrolyte can be detected with higher accuracy and higher probability than by using a thermometer or conductivity meter alone.

Optimization of electrolytes for batteries still requires a trial-and-error approach, even when design of experimental methods is used. These methods strongly reduce the number of samples prepared when the battery electrolytes are optimized. With these methods, reductions of the number of samples from a few thousand to less than 30 samples per optimization run can be achieved. The remaining number of samples is still too high if specific conductivity is to be measured with standard equipment. The multichannel equipment described here speeds up electrolyte development because the remaining number of samples can be analyzed in a short period of time.

Because of the high resolution of both the thermometer and the conductivity meter, supercooling phenomena of electrolytes and ILs can be analyzed in detail. This is especially important for the investigation of the temperature dependence of ILs, because these unconventional solvents are prone to supercooling,[12] which falsifies the outcome of the measurement when it occurs.

### Acknowledgment

We thank Prof. Dr. Josef Barthel for introducing us to fundamental research in the field of the physical chemistry and electrochemistry of electrolyte solutions. The studies of our work group, Electrochemistry and Electrolytes, are based on his previous work and inspired by his continuous interest. The authors also thank H. Becker for discussions and D. Moosbauer, M. Amereller, and A. Schweiger for editing assistance.

### Supporting Information Available:

(1) A detailed description of the in-house-built equipment, including descriptions of the measurement cells (1.1), stirring

equipment (1.2), thermostat (1.3), and thermometer (1.4); (2) a detailed description of the circuitry of the conductivity meter, including information on the sine generator (2.1), voltage divider (2.2), rectification (2.3), analog-to-digital converter (2.4), additional circuitry (2.5), synchronous control of the thermometer and conductivity meter (2.6), and software (2.7); (3) a rigorous error discussion based on the error propagation law; (4) a noise study; and (5) related references. This material is available free of charge via the Internet at http://pubs.acs.org.

## Literature Cited


(1) Broadhead, J.; Kuo, H. C. In *Handbook of Batteries*, 2nd Ed.; Linden, D., Ed.; McGraw-Hill: New York, 1995; Chapter 2, p 2.2.

(2) Salomon, M.; Lin, H. P.; Plichta, E. J.; Hendrickson, M. In *Advances in Lithium Ion Batteries*; von Schalkwijk, W., Scrosati, B., Eds.; Kluwer Academic: New York, 2002; Chapter 11, pp 309−344.

(3) Barthel, J.; Gores, H. J., in *Handbook of Battery Materials*; Besenhard, J. O., Ed.; VCH: New York, 1998; Chapter 7, pp 457−497 and literature cited therein. A new edition is in preparation.

(4) Barthel, J.; Wachter, R.; Gores, H. J. In *Modern Aspects of Electrochemistry*, Vol. 13; Conway, B. E., Bockris, J. O., Eds.; Plenum: New York, 1979; Chapter 1, pp 1−79.

(5) Gores, H. J.; Multerer, M.; Schweiger, H.-G. In *Advanced Materials and Methods for Lithium Ion Batteries*; Zhang, S. S., Ed.; Transworld Research Network: Kerala, India, 2007; Chapter 11, pp 257−277.

(6) Schweiger, H.-G.; Multerer, M.; Schweizer-Berberich, M.; Gores, H. J. Finding Conductivity Optima of Battery Electrolytes by Conductivity Measurements Guided by a Simplex Algorithm. *J. Electrochem. Soc.* **2005**, *152*, A577–A582.

(7) Ohno, H. *Electrochemical Aspects of Ionic Liquids*; Wiley: Hoboken, NJ, 2005.

(8) Wachter, P.; Schweiger, H.-G.; Wudy, F.; Gores, H. J. Efficient determination of crystallisation and melting points at low cooling and heating rates with novel computer controlled equipment. *J. Chem. Thermodyn.* **2008**, *40*, 1542–1547.

(9) Barthel, J.; Wachter, R. Studies on the temperature dependence of properties of electrolyte solutions. Part II. Conductivity determination over a large temperature range. *Ber. Bunsen-Ges. Phys. Chem.* **1979**, *83*, 634–642.

(10) Schweiger, H.-G.; Multerer, M.; Gores, H. J. Fast Multichannel Precision Thermometer. *IEEE Trans. Instrum. Meas.* **2007**, *56*, 2002–2009.

(11) Nishida, T.; Tashiro, Y.; Yamamoto, M. Physical and electrochemical properties of 1-alkyl-3-methylimidazolium tetrafluoroborate for electrolyte. *J. Fluorine Chem.* **2003**, *120*, 135–141.

(12) Ngo, H. L.; LeCompte, K.; Hargens, L.; McEwen, A. B. Thermal properties of imidazolium ionic liquids. *Thermochim. Acta* **2000**, *97*, 357–358.

(13) Noda, A.; Watanabe, M. Highly conductive polymer electrolytes prepared by in situ polymerization of vinyl monomers in room temperature molten salts. *Electrochim. Acta* **2000**, *45*, 1265–1270.

(14) Noda, A.; Hayamizu, K.; Watanabe, M. Pulsed-Gradient Spin-Echo $^{1}H$ and $^{19}F$ NMR Ionic Diffusion Coefficient, Viscosity, and Ionic Conductivity of Non-Chloroaluminate Room-Temperature Ionic Liquids. *J. Phys. Chem. B* **2001**, *105*, 4603–4610.

(15) Van Valkenburg, M. E.; Vaughn, R. L.; Williams, M.; Wilkes, J. S. Thermochemistry of ionic liquid heat-transfer fluids. *Thermochim. Acta* **2005**, *425*, 181–188.

(16) Yoshida, Y.; Muroi, K.; Otsuka, A.; Saito, G.; Takahashi, M.; Yoko, T. 1-Ethyl-3-methylimidazolium Based Ionic Liquids Containing Cyano Groups: Synthesis, Characterization, and Crystal Structure. *Inorg. Chem.* **2004**, *43*, 1458–1462.

(17) MacFarlane, D. R.; Golding, J.; Forsyth, S.; Forsyth, M.; Deacon, G. B. Low viscosity ionic liquids based on organic salts of the dicyanamide anion. *Chem. Commun.* **2001**, 1430–1431.

(18) Wachter, P.; Schreiner, C.; Zistler, M.; Gerhard, D.; Wasserscheid, P.; Gores, H. J. A microelectrode study of triiodide diffusion coefficients in mixtures of room temperature ionic liquids, useful for dye-sensitised solar cells. *Microchim. Acta* **2008**, *160*, 125–133.

(19) Wachter, P.; Zistler, M.; Schreiner, C.; Fleischmann, M.; Gerhard, D.; Wasserscheid, P.; Barthel, J.; Gores, H. J. Temperature dependence of the non-Stokesian charge transport in binary blends of ionic liquids. *J. Chem. Eng. Data* **2009**, *54*, 491–497.

(20) Wachter, P.; Zistler, M.; Schreiner, C.; Berginc, M.; Krašovec, U. O.; Gerhard, D.; Wasserscheid, P.; Hinsch, A.; Gores, H. J. Characterisation of DSSC-electrolytes based on 1-ethyl-3-methylimidazolium dicyanamide: Measurement of triiodide diffusion coefficient, viscosity, and photovoltaic performance. *J. Photochem. Photobiol., A* **2008**, *197*, 25–33.


Received for review November 1, 2009. Accepted January 4, 2010. This work was supported by the Deutsche Forschungsgemeinschaft (DFG) in association with the “Projekt Initiative PAK 177, Funktionsmaterialien und Materialanalytik zu Lithium-Hochleistungsbatterien” (Contract 544243).

JE900942F